11th International Symposium on Turbulence and Shear Flow Phenomena (TSFP11)
Southampton, UK, July 30 to August 2, 2019

EXPERIMENTAL STUDY OF TURBULENT JETS AND FORCED PLUMES: ENTRAINMENT PROFILE COEFFICIENTS AND PREDICTIONS FROM SOME EXISTING MODELS

Himanshu Mishra
Department of Mechanical Engineering
The University of Melbourne
Victoria 3010, Australia
h.mishra@student.unimelb.edu.au

Jimmy Philip
Department of Mechanical Engineering
The University of Melbourne
Victoria 3010, Australia
jimmyp@unimelb.edu.au

ABSTRACT

Integral models based on entrainment hypothesis have been used for several decades to make growth predictions for turbulent jets and plumes. Although useful, these models are based on ad-hoc assumptions, and say very little about the underlying flow physics. Recently, van Reeuwijk & Craske (2015) derived an energy consistent unified entrainment relation, which separates the contributions from mean and turbulence in velocity, buoyancy and pressure via profile coefficients. Here, we present the results of simultaneous time resolved measurement of velocity and density in an axisymmetric turbulent jet and a forced plume using 2D-2C particle image velocimetry (PIV) and planar laser induced fluorescence (PLIF), respectively; using refractive index matched fluids we remove uncertainties due to optical distortions. We present the variations of profile coefficients in the near field, transition and far-field regimes for both jet and forced plume. We compare the solutions obtained from the classical entrainment models, which make assumptions about the profile coefficients, with the current experiment data. Results show discrepancy between data and model solutions, suggesting the need for improved entrainment models.

Introduction

Understanding turbulent buoyant jets and plumes is central to quantifying the entrainment and mixing processes that occur in a wide range of industrial and natural flows. An accurate prediction of these processes are key for both the optimal design of the waste discharge facilities and the related environmental impact assessment. The factors of prime importance to jets and plume dynamics are the integral volume flux Q, specific momentum flux M, buoyancy B and buoyancy flux F, which are defined as,

$$\begin{aligned} Q &= 2\int_0^\infty \overline{w} r \mathrm{d}r, \;\; M = 2\int_0^\infty \overline{w}^2 r \mathrm{d}r, \\ B &= 2\int_0^\infty \overline{b} r \mathrm{d}r, \;\; F = 2\int_0^\infty \overline{w}\overline{b} r \mathrm{d}r, \end{aligned} \tag{1}$$

where r is the radial direction, w is the axial velocity and b = $g\Delta\rho/\rho$. Here over bar and primes denote mean and fluctuating quantities; (e.g. $w = \overline{w} + w'$). These integral quantities can be used to define local width (r_m), velocity (w_m) and buoyancy (b_m) scales without assuming any shape profiles for $\overline{w}$ and $\overline{b}$ as,

$$r_m = \frac{Q}{M^{1/2}}, \quad w_m = \frac{M}{Q}, \quad b_m = \frac{BQ}{M^2}. \tag{2}$$

Radial integration of Reynolds averaged equations of mass, streamwise momentum, buoyancy and energy conservation results in set of differential equations for Q, M and F,

$$\frac{dQ}{dz} = 2\alpha M^{1/2}, \tag{3}$$

$$\frac{d}{dz}\left(\beta_g M\right) = \frac{FQ}{\theta_m M}, \tag{4}$$

$$\frac{d}{dz}\left(\frac{\theta_g}{\theta_m}F\right) = 0, \tag{5}$$

$$\frac{d}{dz}\left(\gamma_g \frac{M^2}{Q}\right) = \delta_g \frac{M^{5/2}}{Q^2} + 2F. \tag{6}$$

Here, although α is the usual entrainment coefficient defined as ratio of radial velocity at the plume edge to characteristic axial velocity inside the plume, in the above set of equations α could simply be considered as one of the four unknowns. An exact expression for α can be obtained using (3), (4) and (6) as, (van Reeuwijk & Craske (2015))

$$\alpha = -\frac{\delta_g}{2\gamma_g} + \left(\frac{1}{\beta_g} - \frac{\theta_m}{\gamma_g}\right)Ri + \frac{Q}{2M^{1/2}}\frac{d}{dz}\left(\log\frac{\gamma_g}{\beta_g^2}\right) \tag{7}$$

where $Ri \equiv b_m r_m / w_m^2$ is the Richardson number. The parameters β, γ, θ and δ are the profile coefficients corresponding to dimensionless momentum flux, energy flux, buoyancy flux and turbulence production. The gross value of any profile coefficient, e.g., $\beta_g = \beta_m + \beta_f + \beta_p$ is made up of contributions from mean, fluctuation and pressure, respectively. The profile coefficients are defined as (van Reeuwijk & Craske (2015)):

$$\beta_m \equiv \frac{M}{w_m^2 r_m^2} = 1, \qquad \beta_f \equiv \frac{2}{w_m^2 r_m^2}\int_0^\infty \overline{w'^2} r\mathrm{d}r, \qquad \beta_p \equiv \frac{2}{w_m^2 r_m^2}\int_0^\infty -\overline{u'^2} r\mathrm{d}r,$$
$$\gamma_m \equiv \frac{2}{w_m^3 r_m^2}\int_0^\infty \overline{w}^3 r\mathrm{d}r, \qquad \gamma_f \equiv \frac{4}{w_m^3 r_m^2}\int_0^\infty \overline{w}\,\overline{w'^2} r\mathrm{d}r, \qquad \gamma_p \equiv \frac{4}{w_m^3 r_m^2}\int_0^\infty -\overline{w}\,\overline{u'^2} r\mathrm{d}r,$$
$$\delta_m \equiv \frac{4}{w_m^3 r_m}\int_0^\infty \overline{w'u'}\frac{d\overline{w}}{dr} r\mathrm{d}r, \qquad \delta_f \equiv \frac{4}{w_m^3 r_m}\int_0^\infty \overline{w'^2}\frac{d\overline{w}}{dz} r\mathrm{d}r, \qquad \delta_p \equiv \frac{4}{w_m^3 r_m^2}\int_0^\infty -\overline{u'^2}\frac{d\overline{w}}{dz} r\mathrm{d}r, \tag{8}$$
$$\theta_m \equiv \frac{F}{w_m b_m r_m^2}, \qquad \theta_f \equiv \frac{2}{w_m b_m r_m^2}\int_0^\infty \overline{w'b'} r\mathrm{d}r.$$

As the experimental measurement of pressure is difficult, the pressure gradient term in Reynolds averaged streamwise momentum $-\partial p/\partial z$ is replaced by $\partial\overline{u'^2}/\partial z$ as in Hussein *et al.* (1994). This has been shown to be a fairly accurate, being able to capture roughly 80% of total pressure (van Reeuwijk *et al.* (2016)).
By ignoring the contribution of turbulence and pressure and assuming the flow to be self-similar, (3), (4) and (5) reduce to the classic entrainment model proposed by Morton *et al.* (1956) and Morton (1959), henceforth referred to as MTT,

$$\frac{dQ}{dz} = 2\alpha M^{1/2}, \quad \frac{dM}{dz} = \frac{FQ}{\theta_m M}, \quad \frac{dF}{dz} = 0. \tag{9}$$

In classic entrainment models, (9) is solved by parametrising α, either as a constant (MTT) or as a function of local Ri (Priestley & Ball (1955), Fox (1970), henceforth PB),

$$\alpha = \alpha_j - (\alpha_j - \alpha_p)\frac{Ri}{Ri_p}, \tag{10}$$

where, α_j and α_p are entrainment coefficient for pure jet and pure plume and Ri_p is constant far field plume Richardson number. The first term in (7) is equivalent to the α_j in (10). The second term adds the effect of Richardson number for forced and pure plumes (parameterized in (10)) and, the third term includes the effect of flow development en-route to self-similarity. For pure jets and plumes, these simplifications for α are adequate (barring the turbulence contribution) once the flow has become self similar. For forced plumes, however, the profile coefficients as well as α vary with varying Ri. Empirically, the variation in α has been observed to follow PB model of entrainment (Wang & Law (2002),henceforth WL). On the other hand, to authors knowledge, the variations in profile coefficients has been measured only by van Reeuwijk *et al.* (2016); however their DNS domain was restricted to $z/d = 25$, and it was observed that turbulence had not achieved self similarity and profile coefficients had not reached the asymptotic state. In the following sections, we will present a description of the present experimental set-up for simultaneous measurement of time-resolved velocity and density fields through a combined PIV and PLIF. We present the measured profile coefficients and their variation, and also compare the predictions of the two classical entrainment models of MTT and PB with our data.

Experiments

A schematic of the experimental set-up is shown in figure 1. The experiments are conducted in a glass test tank

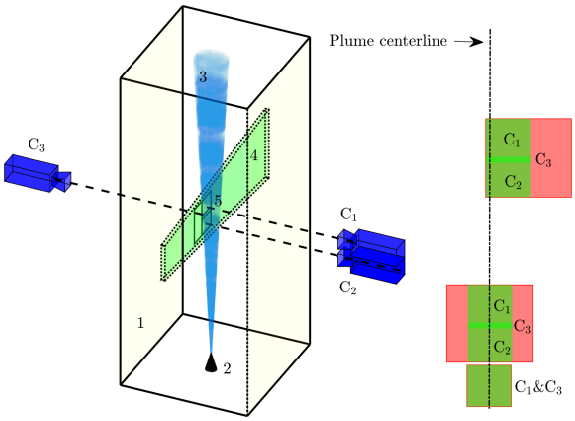

Figure 1. Experimental setup schematic (1) Main glass tank. (2) Nozzle. (3) Plume. (4) Laser. sheet (5) Field of view. C1, C2 represent the two PIV cameras and C3 is the PLIF camera. Right hand side of the figure shows the three locations chosen for measurements in the present experiments. The green color is PIV field of view with overlap between C1 and C2, red color is the PLIF field of view of C3.

(1.2m high and 0.75×0.75 m^2 square base) filled with a solution of water and monopotassium phosphate (the heavy liquid) to a depth of 1m. The side-walls are made of 15mm thick clear glass, and bottom wall constructed from marine grade aluminium is removable, allowing us to change the inlet conditions. A buoyant jet of water and glycerin solution (the light liquid) is driven by a constant-head tank, and discharged from a 3D printed nozzle with exit diameter d = 1cm. The water-glycerin-monopotassium phosphate solution allows us to obtain a constant refractive index and varying density throughout the mixing process. For the jet experiment, water is injected through the nozzle into water-filled tank. Three PCO-dimax HS4 12 bit high speed cameras with 32 GB of RAM were used for the measurements. As PIV provides lower spatial resolution compared to PLIF, two cameras are stacked over each other for PIV, and one was placed on the opposite side of the tank for PLIF. PIV cameras are attached with 105mm lens and 532nm notch filters, whereas PLIF camera is fitted with 60mm lens and 550nm bandpass filter with half width of 25nm. The filters keep the frequencies of scattered laser light out of the PLIF camera and dye fluorescence from the PIV cameras. The same camera configuration is moved vertically for measurements at three different axial locations. The field of view of

Table 1. Experiment parameters. Q_0, M_0, F_0 are initial volume, momentum and buoyancy flux. Initial $Ri_0 = B_0 Q_0 / M_0^{3/2}$ and momentum length scale $l_m = M_0^{3/4}/F_0^{1/2}$. Last two columns are axial measurement locations.

Exp	Q_0 (cm^3/s)	M_0 (cm^4/s^2)	F_0 (cm^4/s^3)	Re_0	Ri_0	l_m (cm)	z/d	z/l_m
J	39.25	1963	0	5000	0	∞	0-7; 8-21; 39-52	-
F	39.25	1963	2311	5000	0.021	6.1	0-7; 8-21; 39-52	0-1.2; 1.2-3.4; 6.4-8.5

the cameras and the axial measurement locations are shown in figure 1. All three cameras are synchronized and operate of 2000×2000 pixels . Flow is illuminated by Spectra Physics 25W and 532nm diode pumped solid state continuous laser. The data processing technique is same as described in Mishra & Philip (2018). Experimental parameters are shown in Table 1, which includes a jet flow and a forced plume at the same initial Reynolds number $Re_0 = d(Q_0/(d^2/4))/\nu$.

Results

Figure 2 shows the instantaneous density overlapped with instantaneous velocity vectors at one axial measurement location.

Figures 3, 4 and 5 show the mean flow, turbulence and pressure profile coefficients for pure jet and forced plume. The largest changes occur over the flow development zone $z/d < 6$. Length of flow developement zone is consistent with the literature as $\approx 5d$ (Papanicolaou & List (1988)) and $\approx$ 6d (WL). For jets, the profile coefficients take a constant value as soon as the flow develops; however, forced plumes behave like jets for $z/l_m \approx 1$ (where $l_m = M_0^{3/4}/F_0^{1/2}$ is the momentum length scale). The forced plume transitions to pure plume above $z/l_m \approx$ 5-6 and hence, profile coefficient take a constant value. Turbulence makes significant positive contribution to the total buoyancy flux of roughly about 20% ($\theta_f \approx 0.2\theta_g$), consistent with the literature (WL). The pressure contribution to the gross profile coefficient (Figure 5) is observed to be negative. This explains why the models which ignore turbulence and pressure contribution, still have been successful in making reasonable prediction of fluxes, especially in case of pure jets and plumes.

Figure 6(a) shows the variation of entrainment coefficient

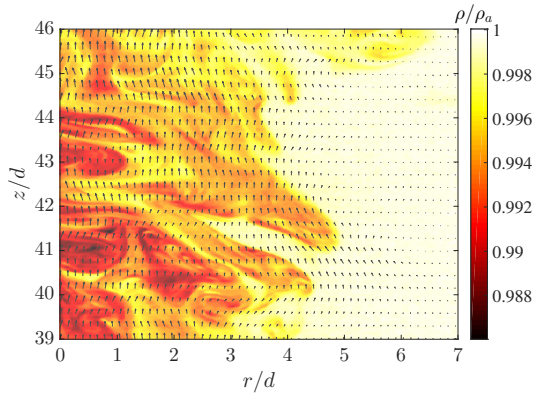

Figure 2. Instantaneous density normalized by ambient density in background, superimposed with velocity vectors (every fifth vector is shown for clarity) at the topmost measurement location. r and z are radial and axial distance from the nozzle.

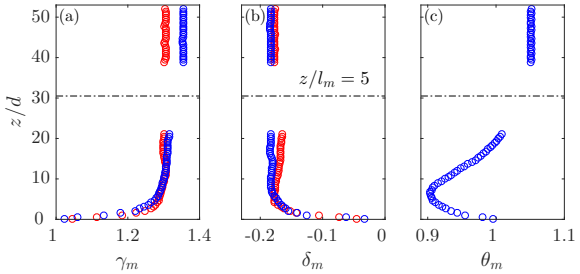

Figure 3. Mean flow contribution to profile coefficients associated with energy flux (γ), turbulence production (δ) and buoyancy (θ).

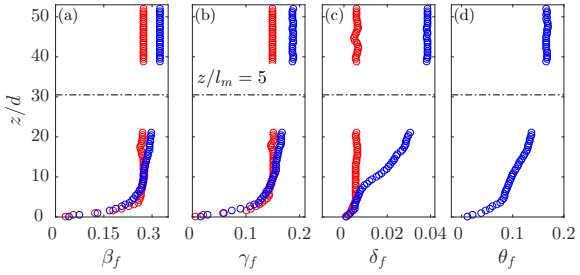

Figure 4. Turbulence contribution to profile coefficients associated with (a) momentum flux (β), (b) energy flux (γ), (c) turbulence production (δ) and (d) buoyancy (θ).

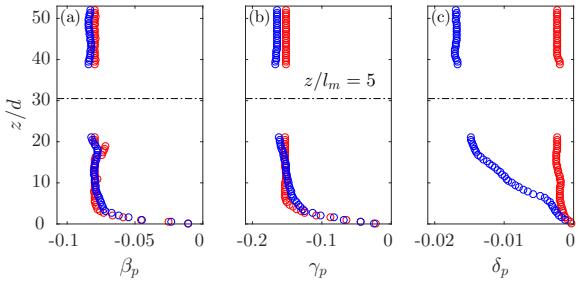

Figure 5. Pressure contribution to profile coefficients associated with (a) momentum flux (β), (b) energy flux (γ) and (c) turbulence production (δ).

for jet (α_j) and forced plume (α_p) with normalized axial distance. α_j quickly reaches a value of 0.052 at $z/d \approx$ 6-7 and, remains roughly constant after that. The value obtained agrees with 0.053 by MTT and 0.0525 by WL. α_p reaches the value of α_j at $z/l_m \approx 1$ and transition to a constant value of 0.087 after $z/l_m \approx$ 5-6. This is similar to 0.082 and 0.0875 proposed by MTT and WL respectively. Similarly in 6(b), Richardson number transitions to a constant value of 0.585, agreeing to 0.58 obtained by WL.

Figure 7 shows the comparison of the present experimental results with existing models by MTT and PB for jets.

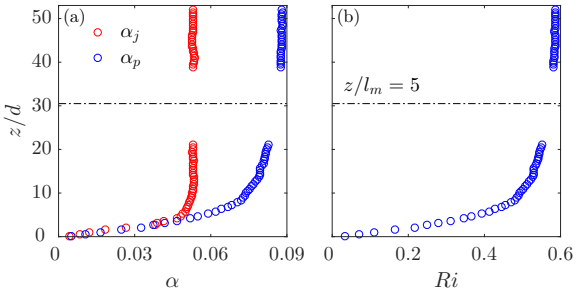

Figure 6. (a) Variation of entrainment coefficient for jet (α_j), forced plume (α_p) and (b) Richardson number with non-dimensionalized axial distance.

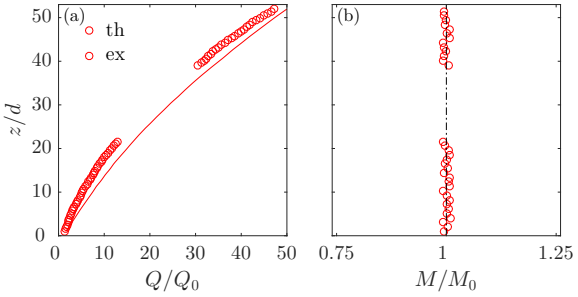

Figure 7. Comparison of experimentally obtained (a) volume flux and (b) momentum flux, with prediction from theory for jet.

As both the models reduce to a constant jet entrainment (cf. equation 10), they are the same in the case of jets. Model prediction is obtained by solving (9) with entrainment coefficient $\alpha_j = 0.053$ given by MTT. The difference between the model prediction and experimental data can be attributed to slightly different entrainment coefficient obtained in the present experiment, and more importantly to the model ignoring turbulence and pressure contribution. Figure 7(b) acts as a validation of the experimental setup, showing the conservation of axial momentum for the jet. Figure 8 shows the comparison of the present experimental results with existing models by MTT and PB for forced plume. MTT model treats α as a constant, assumes self-similarity and ignores turbulence contribution. A constant value of $\alpha_p = 0.082$ is used to solve (9). It can be seen that it over predicts Q and M roughly by a factor of two. This is expected as figure 6 shows that for forced plume the entrainment value transitions from a lower value similar to jet to a higher value for plume. A single large entrainment coefficient would obviously result in over-prediction. PB model provides α varying with Ri as given by (10). Same α_j and α_p as given in MTT are used for solving (9). The predictions are better, especially for Q; however, M prediction do not improve to the same degree as Q. This is because this model also ignores turbulence contribution to buoyancy flux, and hence the increase in M due to turbulence contribution to F is not captured. Although the PB model predictions are comparatively better, it can be seen that self similar assumption and neglecting turbulence and pressure contribution results in incorrect predictions in both cases, being worse in case of forced plume.

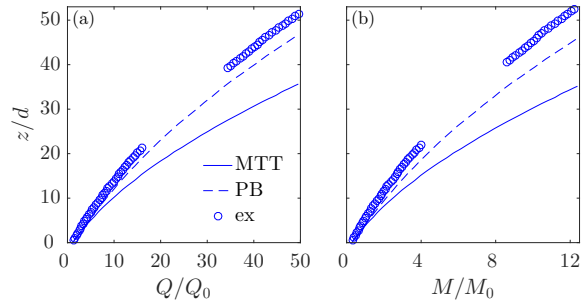

Figure 8. Comparison of experimentally obtained (a) volume flux and (b) momentum flux, with prediction from theory for forced plume.

Conclusion

Simultaneous measurements of velocity and density in a turbulent jet and forced plume is carried out using PIV and PLIF. Near field, transition and pure plume regions are captured to provide a complete description of the evolution of profile coefficients, entrainment and Richardson number. classical entrainment models are solved and compared with the obtained data. It is observed that these models which assume self similarity and do not include turbulence contribution do not accurately predict the fluxes. As all the profile coefficients show a similar behavior of transition from jet to plume with z/l_m in the current experiments, this can be used for their parametrization. The parametrization of profile coefficients also results in a form for α via (7), which can provide a new consistent entrainment model applicable in both near and far field including both turbulence and pressure contribution.

Acknowledgment

The authors gratefully acknowledge the Australian Research Council for the financial support of this work.

REFERENCES

Fox, D.G 1970 Forced plume in a stratified fluid. *Journal of Geophysical Research* **75** (33), 6818–6835.

Hussein, H.J, Capp, S.P & George, W.K 1994 Velocity measurements in a high-reynolds-number, momentum-conserving, axisymmetric, turbulent jet. *Journal of Fluid Mechanics* **258**, 31–75.

Mishra, H & Philip, J 2018 Simultaneous velocity and density measurements using PIV and PLIF in turbulent axisymmetric buoyant plumes. In *Proc. 21st AFMC. Conf*.

Morton, B.R 1959 1959 Forced plumes. *Journal of Fluid mechanics* **5** (1), 151–163.

Morton, B.R, Taylor, G.I & Turner, J.S 1956 Turbulent gravitational convection from maintained and instantaneous sources. *Proceedings of the Royal Society of London. Series A. Mathematical and Physical Sciences* **234** (1196), 1–23.

Papanicolaou, P.N & List, E.J 1988 Investigations of round vertical turbulent buoyant jets. *Journal of Fluid Mechanics* **195**, 341–391.

Priestley, C.H.B & Ball, F.K 1955 Continuous convection from an isolated source of heat. *Quarterly Journal of the Royal Meteorological Society* **81** (348), 144–157.

van Reeuwijk, M & Craske, J 2015 Energy-consistent en-

trainment relations for jets and plumes. *Journal of Fluid Mechanics* **782**, 333–355.

van Reeuwijk, M, Salizzoni, P, Hunt, G.R & Craske, J 2016 Turbulent transport and entrainment in jets and plumes: A dns study. *Physical Review Fluids* **1** (7), 074301.

Wang, H & Law, A.W 2002 Second-order integral model for a round turbulent buoyant jet. *Journal of Fluid Mechanics* **459**, 397–428.